2016

Ursolic acid enhances macrophage autophagy and attenuates atherogenesis

Shuilong Leng
University of South Carolina - Columbia

Stephen Iwanowycz
University of South Carolina - Columbia

Fatma Saaoud
University of South Carolina - Columbia

Junfeng Wang
University of South Carolina - Columbia

Yuzhen Wang
University of South Carolina - Columbia

See next page for additional authors

Ursolic acid enhances macrophage autophagy and attenuates atherogenesis[S]

Shuilong Leng,[1,*,†] Stephen Iwanowycz,[†] Fatma Saaoud,[†] Junfeng Wang,[†] Yuzhen Wang,[†] Ismail Sergin,[§] Babak Razani,[§] and Daping Fan[1,†]

Department of Human Anatomy,* School of Basic Science, Guangzhou Medical University, Guangzhou, Guangdong 510182, People's Republic of China; Department of Cell Biology and Anatomy,[†] University of South Carolina School of Medicine, Columbia, SC 29209; and Cardiovascular Division,[§] Departments of Medicine and Pathology and Immunology, Washington University School of Medicine, St. Louis, MO 63110

Abstract **Macrophage autophagy has been shown to be protective against atherosclerosis. We previously discovered that ursolic acid (UA) promoted cancer cell autophagy. In the present study, we aimed to examine whether UA enhances macrophage autophagy in the context of atherogenesis. Cell culture study showed that UA enhanced autophagy of macrophages by increasing the expression of Atg5 and Atg16l1, which led to altered macrophage function. UA reduced pro-interleukin (IL)-1β protein levels and mature IL-1β secretion in macrophages in response to lipopolysaccharide (LPS), without reducing IL-1β mRNA expression. Confocal microscopy showed that in LPS-treated macrophages, UA increased LC3 protein levels and LC3 appeared to colocalize with IL-1β. In cholesterol-loaded macrophages, UA increased cholesterol efflux to apoAI, although it did not alter mRNA or protein levels of ABCA1 and ABCG1. Electron microscopy showed that UA induced lipophagy in acetylated LDL-loaded macrophages, which may result in increased cholesterol ester hydrolysis in autophagolysosomes and presentation of free cholesterol to the cell membrane. In LDLR$^{-/-}$ mice fed a Western diet to induce atherogenesis, UA treatment significantly reduced atherosclerotic lesion size, accompanied by increased macrophage autophagy. In conclusion, the data suggest that UA promotes macrophage autophagy and, thereby, suppresses IL-1β secretion, promotes cholesterol efflux, and attenuates atherosclerosis in mice.**—Leng, S., S. Iwanowycz, F. Saaoud, J. Wang, Y. Wang, I. Sergin, B. Razani, and D. Fan. **Ursolic acid enhances macrophage autophagy and attenuates atherogenesis.** ***J. Lipid Res.*** **2016.** 57: **1006–1016.**

Supplementary key words lipophagy • inflammation • cholesterol efflux • atherosclerosis

Autophagy is a highly conserved cellular response to stress, in which cellular components are self-consumed and recycled for downstream metabolism (1). Among the three major kinds of autophagy, macroautophagy, microautophagy, and chaperone-mediated autophagy, macroautophagy is the most prevalent form and, thus, commonly referred to as autophagy (2, 3). Over the past decade, research efforts regarding this ancient biological process have been revived due to the realization that alterations in autophagy play crucial pathological roles in many diseases (4, 5) for which current therapeutic means are limited. While many basic aspects of autophagy have been unraveled, little has been translated into clinical benefit, and no autophagy-modulating therapies have been approved for clinical use.

The autophagy process starts with the formation of a double-membrane autophagosome, which engulfs cytoplasmic materials. Autophagosomes are targeted to the lysosomal compartment and single-membrane autolysosomes are generated in which the sequestered cargos are degraded in the highly acidic environment and the resulting simple products are reused (6, 7). There are many molecules involved in autophagy, including Beclin-1 (involved in vesicle nucleation); Atg5, Atg7, and Atg16L1 (involved in vesicle elongation); and LC3 (involved in the expansion of autophagosome membrane and autophagosome-lysosome fusion) (8). Autophagy occurs in almost all cell types, including macrophages. Macrophages primarily use phagocytosis as the first line of defense against exogenous pathogens and endogenous waste products. They adopt autophagy to process bulky materials (e.g., damaged mitochondria and excessive lipids) in unfavorable microenvironments, thus mitigating cytotoxicity. Recently, autophagy has been shown to play a critical role in inflammatory responses in macrophages by interacting with inflammasomes or directly targeting pro-interleukin

This study was supported by Office of Extramural Research, National Institutes of Health Grants HL116626 and AT003961-8455 to D.F., and HL125838 to B.R., and Guangdong Natural Science (2015A030313463 to S.L). The authors declare no financial conflicts of interest. The content is solely the responsibility of the authors and does not necessarily represent the official views of the National Institutes of Health.

Manuscript received 17 December 2015 and in revised form 1 April 2016.

Published, JLR Papers in Press, April 10, 2016
DOI 10.1194/jlr.M065888

Abbreviations: AcLDL, acetylated LDL; CE, cholesterol ester; FC, free cholesterol; IL, interleukin; LD, lipid droplet; LPS, lipopolysaccharide; ORO, Oil Red O; pMΦ, peritoneal macrophage; qPCR, quantitative real-time PCR; TLR, toll-like receptor; UA, ursolic acid.

[1] To whom correspondence should be addressed.
e-mail: shuilongleng@hotmail.com (S.L.); daping.fan@uscmed.sc.edu (D.F.)

[S] The online version of this article (available at http://www.jlr.org) contains a supplement.

(IL)-1β and thereby limiting IL-1β production (9–11). Autophagy, in the form of lipophagy, contributes to macrophage cholesterol homeostasis by cooperating with lysosomes in presenting free cholesterol (FC) for apoAI-mediated cholesterol efflux (12–14). Moreover, when macrophages are doomed to die, macrophage autophagy also appears to play a role in facilitating efferocytosis (a process in which apoptotic cells are phagocytosed and removed) (15, 16).

Lipid-laden macrophages play a crucial role in the initiation of atherogenesis, and inflammatory responses of macrophages are a driving force for atherosclerotic progression and plaque growth (17–21). Unbalanced macrophage foam cell apoptosis and efferocytosis lead to necrotic core formation in advanced plaques and plaque instability (22). Recently, limited but convincing studies have shown that macrophage autophagy is atheroprotective by substantially altering all these aspects, including the enhancement of cholesterol efflux, suppression of inflammation, and improvement of efferocytosis (11, 15, 23). Evidence showing that atherosclerosis progression is accompanied by increasing defects in macrophage autophagy provides further enthusiasm regarding the possibility that enhancement of macrophage autophagy may be an effective way to reduce or reverse atherosclerosis. However, currently known autophagy inducers, including mTOR inhibitors and toll-like receptor (TLR) 7 ligands, are less than ideal therapeutics in the context of atherosclerosis, due to hyperlipidemic (24) and pro-inflammatory effects, respectively (25). Therefore, the search for new macrophage autophagy stimuli is urgent.

Ursolic acid (UA), a natural pentacyclic triterpene carboxylic acid found in various plants, is present in the human diet and possesses a wide range of biological functions, such as anti-oxidation, anti-inflammation (26), anti-cancer (27), and anti-hyperlipidemia (28). Some studies have reported that UA reduces obesity, glucose intolerance, and fatty liver (29, 30). These beneficial properties are of apparent value for the treatment of atherosclerosis, although the underlying molecular mechanisms are largely unknown. Indeed, limited animal studies have shown the potential anti-atherogenic effects of UA (31). Our recent finding that UA promotes cancer cell autophagy (32) prompted us to determine whether this autophagy-enhancing function also holds true in macrophages. To this end, we performed both in vitro and in vivo studies and found that UA enhances macrophage autophagy, suppresses lipopolysaccharide (LPS)-induced IL-1β production and secretion, and promotes cholesterol efflux from acetylated (Ac)LDL-loaded macrophages. Furthermore, we found that UA attenuated atherogenesis in LDLR$^{-/-}$ mice fed a Western diet. Our results suggest that UA may be developed as a new anti-atherogenic agent by virtue of its ability in enhancing macrophage autophagy in an atherogenic environment.

MATERIALS AND METHODS

Materials and reagents

UA ($C_{30}H_{48}O_3$, molecular weight 456.70 Da) was purchased from Changsha Luyuan Bio-Technology Co., Ltd. (Changsha, China). The purity of UA was determined by HPLC as >98% by Dr. Qian Wang at the Department of Chemistry and Biochemistry, University of South Carolina. LPSs, Wortmannin, and bafilomycin were purchased from Sigma-Aldrich (St. Louis, MO). Pam3CSK4 was obtained from Invitrogen (Carlsbad, CA). Rabbit anti-IL-1β antibody (catalog number 12507) and mouse anti-IL-1β antibody (catalog number 12242) were from Cell Signaling Technology (Danvers, MA); rabbit anti-LC3 (catalog number L7543) and rabbit anti-actin antibodies (catalog number A2066) were from Sigma-Aldrich; rabbit anti-ABCA1 antibody (catalog number NB400-105) and rabbit anti-ABCG1 antibody (catalog number 400-132) were from Novus Biologicals (Littleton, CO); HRP-conjugated goat anti-rabbit IgG (catalog number A2315) and goat anti-mouse IgG (catalog number L0312) were from Santa Cruz (Dallas, TX); rat monoclonal MOMA2 (catalog number 3451) was from Abcam Inc. (Cambridge, MA); Alexa Fluor®488-labeled donkey anti-goat IgG (catalog number 1298475) and Alexa Fluor® 555 goat anti-rabbit IgG (catalog number 1683674) were from Life Technologies (Waltham, MA). Primers were synthesized by Invitrogen.

Cell culture and manipulation

RAW264.7 cells were obtained from ATCC (Rockville, MD) and were maintained in DMEM with10% FBS. Thioglycollate-elicited mouse peritoneal macrophages (pMΦs) were obtained as previously described (33) and cultured in DMEM with 10% FBS for 2 h, unattached cells were washed away, and the attached macrophages were then further cultured in appropriate medium. For LPS treatment, pMΦs were incubated for 6–24 h in the culture medium (DMEM with 0.25% FBS) with an addition of LPS and UA at the indicated concentrations. The cells were then washed with Dulbecco's PBS twice before being lysed for total RNA or protein extraction. Raw 264.7 cells and pMΦs were treated with UA (10 μM) and TLR1/2 ligand Pam3CSK4 (500 ng/ml) or TLR4 ligand LPS (100 ng/ml) either alone or in combination, as indicated, for 6 h. In some experiments, cells were exposed to various autophagy modulators for 1 h prior to UA treatment, such as 500 nM Wortmannin to inhibit PI3K or 100 nM bafilomycin to inhibit degradation of LC3.

Mice

All mice were purchased from the Jackson Laboratory (Bar Harbor, ME) and housed in the University of South Carolina Animal Research Facility. All animal experiments were carried out in compliance with the National Institutes of Health guidelines and were approved by the Institutional Animal Care and Use Committee of the University of South Carolina. In the serum IL-1β measurement experiment, C57BL/6 mice were randomly grouped (four mice in the control group, five mice in the LPS group, and five mice in LPS plus UA group) and were injected intraperitoneally with either LPS (20 μg/mouse) alone or together with UA (50 mg/kg), and blood was taken after 16 h for analysis of serum IL-1β by ELISA using kits from eBioscience (catalog number BMS6002INST; San Diego, CA). For atherosclerosis studies, female LDLR$^{-/-}$ mice were fed a Western diet and treated with UA for 11 weeks before they were euthanized for analysis. The Western diet contained 21% (wt/wt) anhydrous milkfat, 34% (wt/wt) sucrose, and a total of 0.2% (wt/wt) cholesterol (diet number TD.88137; Harlan Laboratories, Indianapolis, IN).

MTT assay

The pMΦs were cultured in phenol red-free medium in 24-well plates. Cytotoxicity of UA was determined using an MTT cell viability assay kit from ATCC Bioproducts™ (Manassas, VA) following the manufacturer's instructions. The 96-well microplates were read using a SpectraMax M5 microplate reader (Molecular Devices, Sunnyvale, CA); absorbance at 570 nm was measured.

Macrophage cholesterol efflux

The cholesterol efflux assay was processed as previously described (34). Attached mouse macrophages in 24-well plates were cultured in DMEM for 24 h followed by cholesterol-loading with 100 μg/ml AcLDL incorporated with ^{3}H-cholesterol for 3 days. Then efflux medium (either FBS-free DMEM or DMEM containing 20 μg/ml human apoAI or 50 μg/ml human HDL) with the absence or presence of 10 μM UA was added to initiate cholesterol efflux for 24 h. ^{3}H radioactivity in efflux medium and cells was counted using a Beckman LS6500 liquid scintillation counter (Beckman Coulter, Indianapolis, IN). Cholesterol efflux rate was calculated as the percentage of the radioactivity counts in the medium. ^{3}H-labeled cholesterol was purchased from Perkin-Elmer (Waltham, MA). AcLDL and human HDL were from Biomedical Technologies (Stoughton, MA).

Quantitative real-time PCR

Total RNA was extracted using TRIzol reagent (Invitrogen, San Diego, CA) and reverse transcribed into cDNA using iScript™ Reverse Transcription Supermix (Bio-Rad Laboratories, Inc., Hercules, CA). Quantitative real-time PCR (qPCR) analysis was carried out using iQ™ SYBR® Green Supermix (Bio-Rad) on an Eppendorf Realplex2 mastercycler (Eppendorf, Hamburg, Germany). The primers used in qPCR were: mouse 18S RNA (internal control), 5′-CGCGGTTCTATTTTGTTGGT-3′(forward) and 5′-AGTCGGCATCGTTTATGGTC-3′(reverse); mouse IL-1β, 5′-GCCCATCCTCTGTGACTCAT-3′ (forward) and 5′-AGGCCACAGGTATTTTGTCG-3′ (reverse); mouse BECN1, 5′-GGCCAATAAGATGGGTCTGA-3′ (forward) and 5′-GCTGCACACAGTCCAGAAAA-3′ (reverse); mouse Atg16l1, 5′-GGTGCCGTAGCTTTCTTGAG-3′ (forward) and 5′-ACTGTGTCCAGTGGGGAGAC-3′ (reverse); mouse Atg4c, 5′-GCATTCCTGTTTCCCAAAGA-3′ (forward) and 5′- AAACCCGAAAGTCCTCTGGT-3′ (reverse); mouse Atg5, 5′-AGATGGACAGCTGCACACAC-3′ (forward) and 5′-GCTGGGGGACAATGCTAATA-3′ (reverse). Samples were amplified using the following program: 95°C for 10 min followed by 40 cycles of 95°C for 10 s, 60°C for 15 s, and 68°C for 20 s, and then a melting curve analysis from 60 to 95°C every 0.2°C. The abundance of each gene product was calculated by relative quantification, with values for the target genes normalized with 18S RNA.

Western blot

Protein samples were loaded onto SDS-PAGE gels for electrophoresis. The size-separated proteins were then transferred to nitrocellulose membranes (Amersham Biosciences, Piscataway, NJ). The indicated primary antibodies and HRP-conjugated secondary antibodies were used to detect target proteins. Signal was detected using an ECL kit (Bio-Rad). For stripping, membranes were submerged for 30 min at 55–60°C in a buffer containing 100 mM 2-mercaptoethanol, 2% (v/v) SDS and 62.5 mM Tris-HCl (pH 6.7), with agitation, and then were washed three times with PBST.

Measurement of cytokines in cell culture medium or serum

Cytokine protein concentrations in cell culture medium or serum were measured by ELISA, using kits from eBioscience (San Diego, CA) following the manufacturer's instructions. The macrophage-conditioned culture medium was diluted by 30- to 180-fold for the measurement. The 96-well microplates were read using a SpectraMax M5 microplate reader.

Immunofluorescence staining

Macrophages were seeded in 8-well chamber slides. Cells were fixed with 4% paraformaldehyde for 3 min at room temperature and permeabilized for 10 min with Triton X-100 (0.1% in PBS). All subsequent steps were conducted at room temperature. The cells were blocked with 0.01 M glycine/PBS three times, 30 min each time, and then with 5% BSA in PBS for 1 h and stained with primary antibody (rabbit anti-LC3 or goat anti-IL-1β at 1:200 in blocking buffer) for 1 h. After washing three times with PBS, the cells were stained with Alexa Fluor 555-conjugated goat anti-rabbit IgG (1:500 in PBS) and with Alexa Fluor 488-conjugated donkey anti-goat IgG (1:500 in PBS) for 1 h. The cells were stained with 4′,6-diamidino-2-phenylindole (5 μg/ml) for 5 min and then washed with PBS. The coverslips were mounted onto glass slides with fluorescent mounting medium (Dabco) and analyzed on an Olympus FV1000 laser scanning confocal microscope (Tokyo, Japan).

Transmission electron microscopy

Cells were cultured on Permanox four chamber slides for different lengths of time. Cells were fixed with 1–2% glutaraldehyde for 30 min and then rinsed with PBS three times; they were then incubated in 1% osmium tetroxide with 1.5% potassium ferricyanide for 30 min and then rinsed with water. The cells were dehydrated by incubating them in 70% ethanol for 15 min twice, then 95% ethanol for 15 min twice, and finally 100% ethanol for 20 min. The cells were then incubated in ethanol and acetonitrile (1:1) for 10 min, then with acetonitrile for 10 min twice; next they were incubated in PolyBed 812 and acetonitrile (1:2) for 1 h, then with PolyBed 812 and acetonitrile (2:1) for 1 h, and within pure PolyBed 812 overnight. Cells were embedded in mold 48 h at 60°C, which was cut and examined by transmission electron microscopy; 50 cells in each group were examined.

Cellular cholesterol analysis

The intracellular total cholesterol and FC were measured by an intracellular cholesterol quantitation kit (Sigma-Aldrich) according to the manufacturer's instructions. Briefly, macrophages were trypsinized with trypsin-EDTA followed by centrifugation. The cell pellets were resuspended in a mix of chloroform:isoporpanol:IGEPAL CA-630 (7:11:0.1). The samples were centrifuged at 13,000 *g* for 10 min to remove insoluble material. The organic phase was transferred to new tubes and air dried at 50°C for 30 min, followed by blowing the samples with nitrogen to remove organic solvent. The lipid was dissolved with 200 μl cholesterol assay buffer; 50 μl of the reaction mix was added to each standard and sample well in a 96-well plate and incubated for 60 min at 37°C in the dark. The absorbance at OD 570 nm was measured with a Spectra Max M5 microplate reader (Molecular Devices).

Plasma lipid analysis

Blood was obtained from mice following an overnight fast and the plasma was obtained by centrifugation of the blood at 4,000 *g* for 20 min. Plasma cholesterol and triglyceride levels were measured by enzymatic colorimetric assays with cholesterol reagent and triglycerides GPO reagent kits (Raichem, SanDiego, CA). Plasma cholesterol lipoprotein profiles were determined using a fast-performance LC system (AKTA purifier, GE Healthcare Biosciences, Pittsburgh, PA) equipped with a Superose 6 10/300 GL column (GE Healthcare). Pooled mouse plasma (100 μl) was loaded onto the column and eluted at a constant flow rate of 0.5 ml/min with 1 mM sodium EDTA and 0.15 M NaCI. Fractions of 0.5 ml were collected and cholesterol concentration from each fraction was measured.

Atherosclerosis analysis

Hearts and aortas were dissected from mice and processed as described previously (35). The base of the heart containing the

aortic root was embedded in OCT medium and frozen at −20°C. The aorta (from the ascending region to the abdominal region) was fixed in 10% neutral buffered formalin at room temperature overnight and then kept in PBS before removing the adventitia. For analysis of atherosclerosis in the aortic root, 10 μm serial sections were collected. Atherosclerotic lesion areas of 10 serial sections were visualized with hematoxylin and eosin staining (hematoxylin: GeneTex, Inc., ready-to-use, catalog number GTX73341; eosin: Sigma-Aldrich, eosin B, catalog number 861006-10G), and lipid-stained lesions were visualized by Oil Red O (ORO) staining and quantified by Image-Pro Plus 6.0. Rat anti-mouse moma2 (Abcam) was used for immunostaining for macrophage analysis on serial sections of the aortic root, and biotinylated goat anti-rabbit IgG (Vector Laboratories, Burlingame, CA; catalog number BA-1000) was used as the secondary antibody. Immunoreactivity was amplified using the Vectastain ABC kit (Vector Laboratories, catalog number PK6100), and signal was enhanced by peroxidase enhancer (GeneTex, Irvine, CA; GTX82979) and finally reacted with the substrate from AEC Chromogen/FRP substrate kit (GeneTex; GTX82977). For collagen staining of the lesions, the 10 μm-thick aortic root sections were stained by Movat's pentachrome using a Movat pentachrome stain kit from Scytek Laboratory (catalog number MPS-2; Logan, UT) following the manufacturer's instructions, and visualized and analyzed by a Nikon NiU research microscope equipped with a NIS-Elements software package and a high resolution CMOS color camera as well as Image-Pro Plus 6.0. The en face aortas were stained with ORO and the plaque areas were analyzed by ImageJ.

Statistical analysis

All data were summarized as mean ± SEM. To compare two groups on a continuous response variable (e.g., gene expression levels and atherosclerosis size), we used a *t*-test. To compare multiple groups on a continuous response variable, we used a one-way ANOVA followed by Bonferroni post assay to compare the selected two groups. Normality and homoscedasticity were tested to ensure that parametric testing was appropriate. $P \leq 0.05$ was considered statistically significant. GraphPad Prism 5 software was used to carry out all statistical analysis.

RESULTS

UA enhances macrophage autophagy

The structure of UA was confirmed by NMR; the purity was determined by mass spectroscopy and HPLC to be >98% (data not shown). Its cytotoxicity was measured by MTT assay. UA was dissolved in DMSO as a stock solution of 10 mM and then diluted into appropriate media. Mouse pMΦs and Raw264.7 cells were treated with 0–40 μM UA for up to 5 days. Data showed that at concentrations up to 10 μM, UA did not cause any apparent cytotoxicity to both cell types, but it led to cell death at >30 μM (data not shown). Therefore, we used UA at 10 μM or lower for all the following experiments. To examine whether UA increases macrophage autophagy, we treated mouse pMΦs with UA and Wortmannin (an autophagy inhibitor). UA-enhanced autophagy was evidenced by increased LC3-I/II proteins, whereas Wortmannin completely blocked UA-induced LC3 increase (**Fig. 1A**). Next, using Raw264.7 cells, we confirmed UA's autophagy-inducing activity. Data showed that UA at 10 μM was 2-fold more effective in increasing LC3I/II expression than rapamycin at 100 nM (Fig. 1B).

The autophagy-enhancing effect of UA was also evident as observed by electron microscopy. As shown in Fig. 1C, UA-treated pMΦs had numerous double-membrane structures that were characteristic of nascent autophagosomes, autophagosomes, and autolysosomes, while much fewer of these structures were detected in control cells. Autophagosomes and nascent autophagosomes could not be clearly distinguished in the micrographs. The structure indicated as "autophagosomes" could also be nascent autophagosomes. In autolysosomes, the segregated organelles lose their distinct shape and are usually replaced by electron-dense materials. The diameter of typical autophagosomes or autolysosomes is 0.5–2 μm. These electron microscopy data have confirmed that UA induces autophagy in pMΦs.

To examine the mechanisms by which UA enhances macrophage autophagy, qPCR was performed and showed that in both mouse pMΦs and Raw264.7 cells, UA at 10 μM significantly increased the expression of autophagy-related proteins Atg5 and Atg16L1, but not that of Atg4c and Beclin-1 (BECN1) (Fig. 1D, E). UA did not change LC3 mRNA expression in macrophages either (data not shown).

UA suppresses IL-1β production in macrophages

It has been reported that UA has anti-inflammatory effects on macrophages (26). To investigate the effects of UA on pro-inflammatory cytokines such as IL-1β, IL-6, and TNFα, pMΦs were treated with LPS (100 ng/ml) and/or UA (10 μM) for 6 h, and the expression of the abovementioned cytokines was examined using qPCR. As shown in **Fig. 2A** and supplementary Fig. 1A, LPS significantly increased the mRNA expression of IL-1β, IL-6, and TNFα; UA only slightly (without statistical significance) suppressed LPS-induced expression of these cytokines. However, Western blot analysis showed that UA substantially reduced the pro-IL-1β protein level in both LPS-treated pMΦs and Raw264.7 cells (Fig. 2B).

We next examined whether UA suppresses mature IL-1β secretion. Mouse pMΦs were treated with LPS or Pam3CSK4 with or without UA for 16 h and the conditioned medium was collected for ELISA measurement of IL-1β protein levels. The result showed that LPS and Pam3CSK4 stimulated the secretion of IL-1β, whereas UA significantly inhibited the secretion of IL-1β (Fig. 2C). However, UA did not significantly reduce the secretion of IL-6 or TNFα in LPS-treated mouse pMΦs (supplementary Fig. 1B).

To determine whether UA suppresses IL-1β production in vivo, we injected C57BL/6 mice intraperitoneally with either PBS (control), LPS alone, or LPS together with UA (50 mg/kg). Sixteen hours after injection, blood samples were taken for analysis of serum IL-1β concentration by ELISA. The results showed that LPS significantly increased serum IL-1β levels and UA significantly suppressed the induction (Fig. 2D). We developed a method to measure mouse serum UA concentration by coupling HPLC

JOURNAL OF LIPID RESEARCH ASBMB JLR

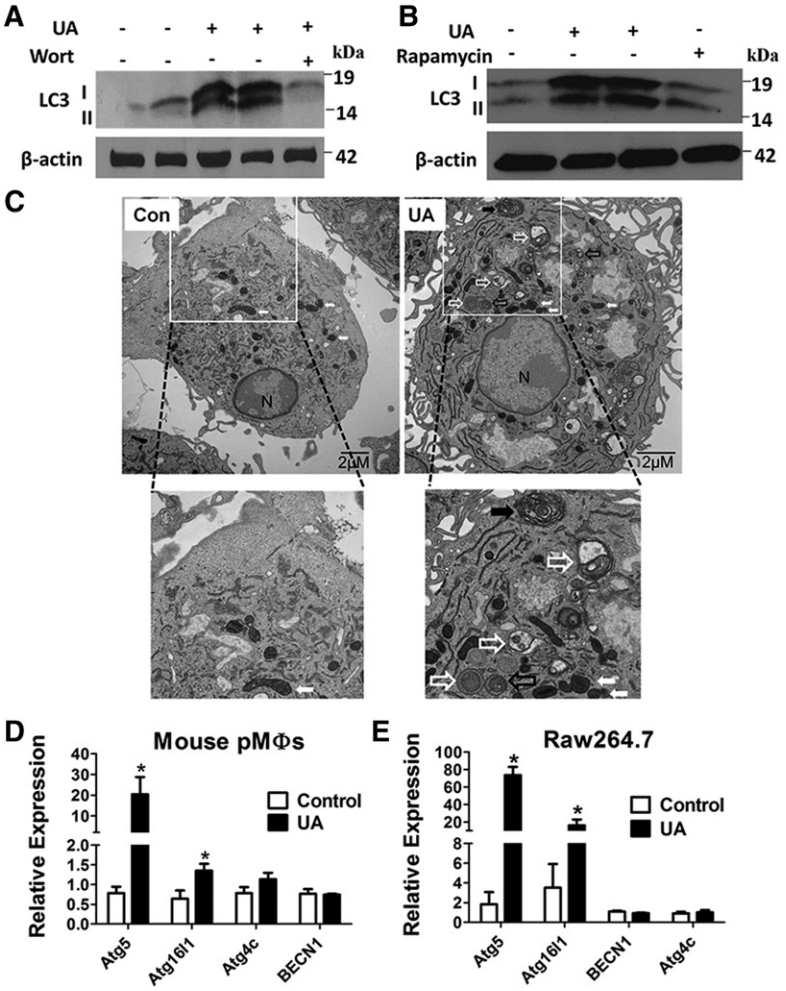

Fig. 1. UA enhances macrophage autophagy. A: Western blot analysis of LC3 in cell lysates from pMΦs treated with UA (10 μM) and Wortmannin (Wort, 500 nM) for 6 h. B: Western blot analysis of LC3 in cell lysates from Raw264.7 cells treated with UA (10 μM) or rapamycin (100 nM) for 6 h. C: Electron microscopy images of pMΦs treated with control (Con) medium or UA (10 μM). pMΦs were treated with UA (10 μM) for 6 h and fixed for electron microscopy as described in the text. Black hollow arrows indicate nascent autophagosomes; white hollow arrows indicate autophagosomes; black solid arrow indicates an autolysosome; white solid arrows indicate mitochondria; N indicates nucleus. Scale bar indicates 2 μm. D, E: The effects of UA (10 μM) on the expression of autophagy-related genes in pMΦs (D) or Raw264.7 cells (E) treated for 6 h. $^*P < 0.05$ versus control.

and mass spectroscopy; we found, after injection of UA at 50 mg/kg, that serum UA concentration peaked at 12 μM at 2 h post injection and dropped to below 3 μM at 24 h post injection (data not shown).

A previous study demonstrated that autophagy inhibits inflammasome activation and IL-1β secretion in response to endotoxin (9). IL-1β is produced by activated macrophages as a proprotein (pro-IL-1β), which is proteolytically processed to its active form by caspase 1. Inflammasome activation results in increased availability of caspase 1 and, therefore, accelerated process of pro-IL-1β. Interestingly, we found that UA did not change the expression of caspase 1 (data not shown). Other studies have shown that, in macrophages, autophagy may also regulate IL-1β secretion by encapsulating and degrading pro-IL-1β in autolysosomes (10). To examine whether UA promotes autophagic sequestration and degradation of pro-IL-1β, we incubated Raw264.7 cells with UA and LPS, and detected the intracellular location of IL-1β and LC3 by confocal microscopy. As shown in Fig. 2E, when Raw264.7 cells were treated with LPS for 24 h, IL-1β staining in the cytosol was significantly greater compared with control; UA-treated cells had dramatically more autophagosomes (LC3 staining) than control or LPS-treated cells. When the cells were treated with LPS and UA, IL-1β staining became weaker and appeared to be colocalized with LC3. The overlap between IL-1β and LC3 signals indicates that autophagy induced by UA may sequester pro-IL-1β in autophagic vesicles.

UA promotes cholesterol efflux from lipid-loaded macrophages

Autophagy has been shown to enhance cholesterol efflux to apoAI (12–14). To examine whether UA promotes macrophage cholesterol efflux by enhancing autophagy, we used mouse pMΦs to perform experiments using previously established protocol (35). We found that UA (10 μM) significantly increased cholesterol efflux to apoAI, but not to HDL (**Fig. 3A**). An autophagic flux inhibitor, bafilomycin A1, completely diminished the cholesterol efflux enhancement by UA (Fig. 3B). qPCR and Western blots showed that UA did not increase the mRNA expression and protein levels of ABCA1 and ABCG1 (Fig. 3C, D), indicating that the cholesterol efflux enhancing effects of UA are not caused by ABCA1 or ABCG1 induction.

To search for evidence of autophagic vacuoles in lipid-loaded macrophages and, if present, whether these were associated with lipid droplets (LDs), electron microscopic analysis was performed. The results clearly showed that UA increased lipophagy in AcLDL-loaded macrophages (Fig. 3E). LDs were easily identifiable as round light-density structures in AcLDL-loaded cells [Fig. 3E(b), white

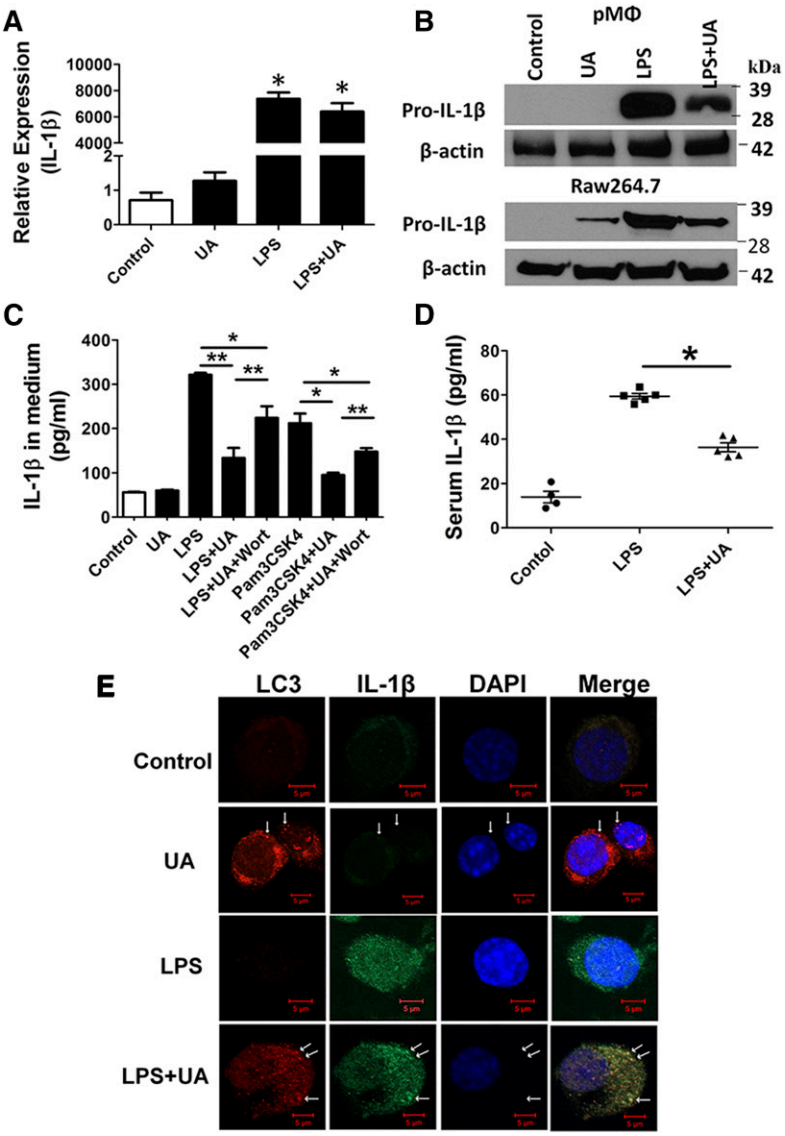

Fig. 2. UA suppresses IL-1β secretion from macrophages via enhancing autophagy. A: UA did not inhibit LPS-induced IL-1β mRNA expression in mouse pMΦs. $*P \leqslant 0.05$ versus control or UA. B: UA reduced pro-IL-1β protein levels in macrophages. C: UA reduced mature IL-1β secretion from macrophages. $*P \leqslant 0.05$; $**P \leqslant 0.01$. D: UA treatment reduced serum IL-1β levels in LPS-treated mice. LPS (20 μg per mouse, ip injection) increased the IL-1β level in serum in mice and UA (50 mg/kg, ip injection) significantly blunted the increase. $*P \leqslant 0.05$. E: Confocal microscopy of Raw264.7 cells treated with UA (10 μM) and/or LPS (100 ng/ml). Arrows point to LC-3 staining. Yellow dots (in merge image of LPS+UA group) indicate colocalization of red (LC-3) and green (IL-1β) signals in Raw264.7 cells. Scale bar: 5 μm.

solid arrow] and UA reduced the number of LDs and increased the frequency of LDs with areas of high density and asymmetrically localized multi-membrane structures, indicating that autophagosomes occur on the surface of the LDs [Fig. 3E(c), black solid arrow].

To examine whether UA increases cholesterol ester (CE) hydrolysis through enhancing autophagy, we measured total cholesterol and FC in mouse pMΦs loaded with 50 μg/ml AcLDL in the absence or presence of 10 μM UA in serum-free DMEM for 24 h; and the CE and FC/CE ratio were calculated. We found that, while UA did not significantly reduce total cholesterol loading to the macrophages, it significantly increased the FC/CE ratio (Fig. 3F), indicating that UA, indeed, increased CE hydrolysis in macrophages.

UA attenuates atherogenesis in hypercholesterolemic mice

Because UA was shown to suppress macrophage IL-1β production and secretion and enhance macrophage cholesterol efflux, we next examined whether UA treatment could reduce atherosclerosis in mouse models. Female $LDLR^{-/-}$ mice at an age of 8 weeks were randomly divided into two groups (9–10 mice per group) and fed a Western diet for 11 weeks. In the DMSO group, the mice were injected intraperitoneally with vehicle (0.1% DMSO in 1 ml PBS) every other day; while in the UA group, the mice were injected with UA (50 mg/kg in 1 ml PBS with 0.1% DMSO) every other day. Food intake and body weight were measured weekly. We noticed that, while the food intake was not different between the two groups (supplementary Fig. 2A), the body weights of the UA group mice were lower than the vehicle group in the first 3 weeks after the initiation of Western diet and UA treatment, but they caught up in the following weeks; at the endpoint, body weights of the two groups were not significantly different (supplementary Fig. 2B). The mice were euthanized and comprehensive analyses were performed to compare the two groups. We did not find any significant differences between the two groups of mice in total serum cholesterol (supplementary Fig. 2C), triglycerides (supplementary Fig. 2D), and fasting blood glucose (supplementary Fig. 2E),

JOURNAL OF LIPID RESEARCH

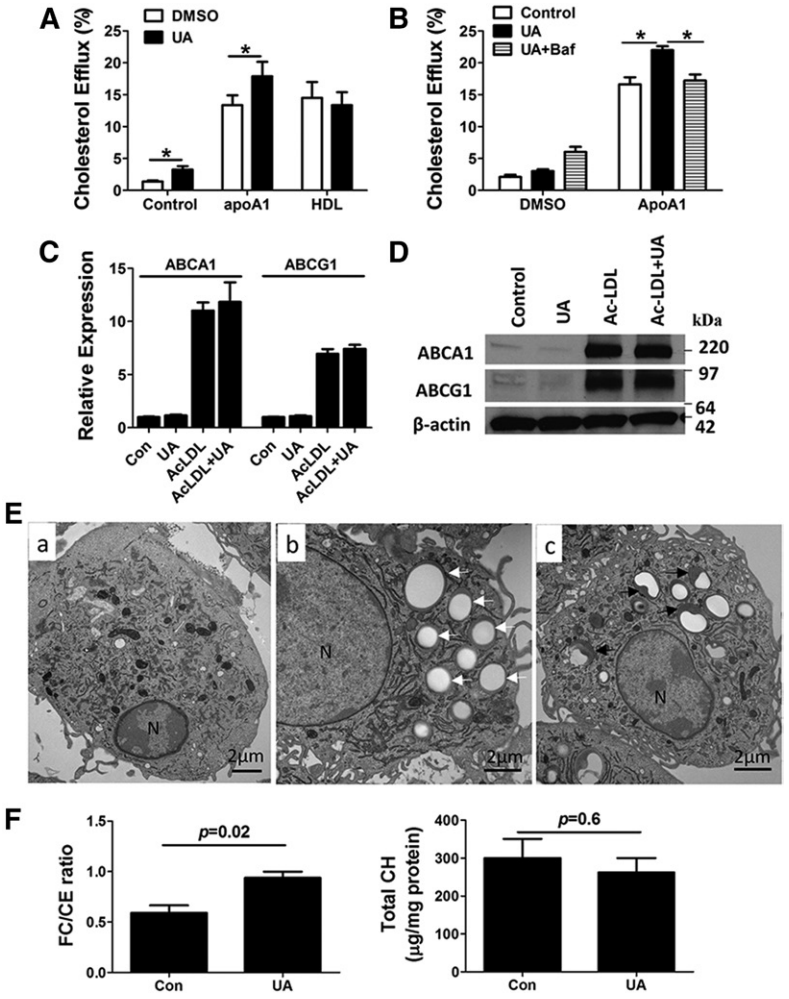

Fig. 3. UA enhances macrophage cholesterol efflux through inducing lipophagy. A: Effects of UA (10 μM) on pMΦ cholesterol efflux to DMEM (Control), apoAI, or HDL. Values are presented as mean ± SEM relative to DMSO control. $*P < 0.05$. B: The effect of UA on macrophage cholesterol efflux to apoAI was diminished by bafilomycin A1 (Baf). $*P < 0.05$. C, D: UA did not affect ABCA1 and ABCG1 mRNA expression (C) and protein levels (D) in cholesterol-loaded pMΦs. pMΦs were loaded with AcLDL, with or without UA, ABCA1, and ABCG1 mRNA and protein levels were determined by qPCR or Western blot. Values are presented as mean ± SEM relative to vehicle control. E. Transmission electron microscopy images of pMΦs: control (a); AcLDL (b); AcLDL+UA (c). White arrows, LDs; black arrows, LDs with areas of high density and asymmetrically localized multi-membrane structures; N, nucleus. Scale bar: 2 μm. F: Total cellular cholesterol and FC/CE ratio were measured for mouse pMΦs loaded with AcLDL for 24 h in the absence or presence of UA.

as well as overall fast-performance LC lipoprotein profile (supplementary Fig. 2F, G). ELISA showed that IL-1β protein levels were reduced in the serum of the UA group compared with the control group, while the serum levels of IL-5 were not different between the two groups of mice (**Fig. 4A**). Interestingly, serum IL-6 and TNFα levels were also significantly reduced in UA-treated mice (supplementary Fig. 2H). The reduction in these cytokines may be secondary to IL-1β reduction and the resulting reduced chronic systemic inflammation in mice.

The UA group of mice developed significantly less atherosclerosis compared with the vehicle group. As visualized by hematoxylin and eosin staining, mean lesion area in the aortic root was 3.72 ± 0.27 and 6.01 ± 0.58 × 10^5 μm^2 in the UA group and the vehicle group, respectively, reflecting a 38% reduction in the UA group (supplementary Fig. 3A). We further stained the aortic root lesions for neutral lipid with ORO. The results showed that the lipid staining area in the lesions of the UA group (3.91 ± 0.31 × 10^5 μm^2) was significantly smaller than that in the vehicle group (5.79 ± 0.22 × 10^5 μm^2), with a 32% reduction (Fig. 4B). We stained lesional macrophages using a mouse macrophage-specific antibody, MOMA-2, and found that the UA group displayed a slightly lower percentage of macrophage area in aortic root atherosclerotic lesions compared with the vehicle group (63.4 ± 2.6% vs. 70.2 ± 2.7%), but without statistical significance (Fig. 4C). However, the collagen content (percentage) in the lesions, as determined by Movat's pentachrome staining, was significantly larger in the UA group (22.9 ± 2.0%) than in the vehicle group (14.7 ± 2.6%) (Fig. 4D). Furthermore, the atherosclerotic lesion area in en face aortas was significantly smaller in the UA group than in the vehicle group (supplementary Fig. 3B, C).

We also stained IL-1β and LC-3 in the aortic root slides to examine whether UA induced autophagy and reduced IL-1β in atherosclerotic lesions. The autophagy levels (reflected by LC-3 staining) in atherosclerotic lesions were increased in the UA group compared with the control group, especially in the macrophage-rich lesions. Meanwhile, the positivity of IL-1β was significantly decreased in the atherosclerotic lesions of the UA group compared with the control group. More interestingly, in the lesions of the UA group, there was significantly more IL-1β and LC-3 overlapping (**Fig. 5**). Our results suggested that UA treatment has increased autophagy in the atherosclerotic lesion, as well as pro-IL-1β degradation in the autophagosome.

DISCUSSION

In this study, we demonstrate that a phytonutrient, UA, enhances macrophage autophagy, suppresses macrophage

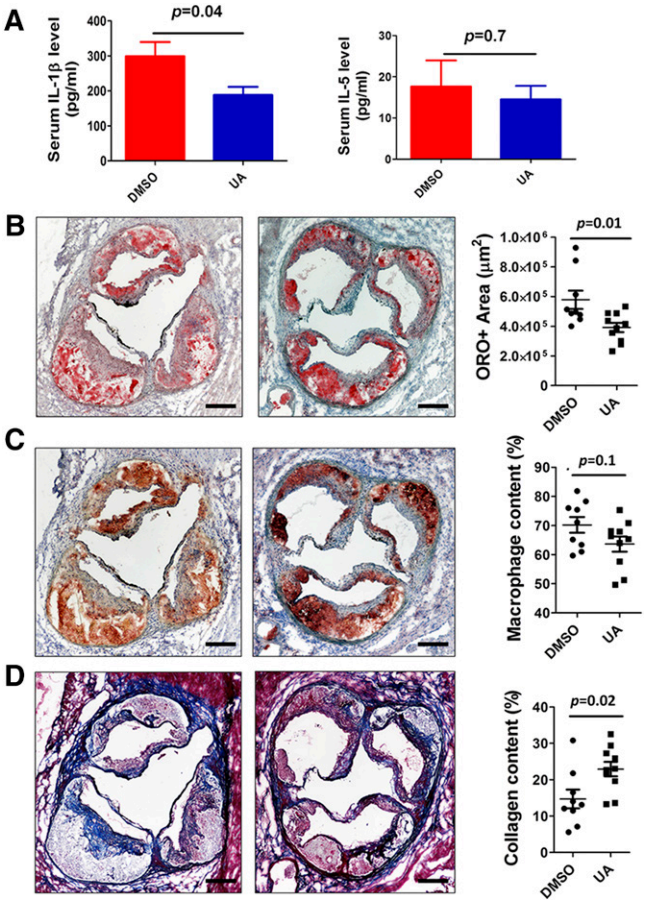

Fig. 4. UA attenuates atherosclerosis in LDLR-deficient mice fed a Western diet. The mice were fed a Western diet for 11 weeks and administered vehicle or UA as described. The aortic roots were embedded in OCT medium and frozen at −20°C immediately after being cut away from the aorta. For analysis of atherosclerosis, 10 micron-thick sections were collected in the region of the proximal aorta, starting from the end of the aortic sinus. A: UA significantly reduced serum IL-1β levels, but did not significantly alter serum IL-5 levels in the mice. B: The lipid content in lesions was determined by ORO staining and quantified by Image-Pro Plus 6.0. The quantitative analysis and representative images are shown. C: The areas of macrophages in lesions were determined by immunostaining for MOMA-2 (a macrophage marker). D: Trichrome staining for quantification of the lesion collagen content. Quantitative analysis and representative images are shown. Scale bar: 250 μm.

IL-1β secretion, and promotes cholesterol efflux from cholesterol-loaded macrophages. Furthermore, we show that administration of UA attenuates atherogenesis in hyperlipidemic mouse models. This represents the first report that a natural compound suppresses atherosclerosis through a mechanism that is associated with macrophage autophagy enhancement.

Several recent studies have convincingly shown that macrophage autophagy plays a protective role against atherogenesis in mouse models. However, using macrophage autophagy induction as an anti-atherosclerosis strategy is a distant goal because none of the known autophagy inducers or enhancers have been shown to be beneficial without reasonable side effects in preclinical studies. For example, systemic administration of mTOR inhibitors at levels sufficient for autophagy induction in macrophages causes systemic immunosuppression. The characterization of UA as a macrophage autophagy inducer in this study may add this natural compound as a new compound for clinical development toward a new anti-atherogenic agent. We show that UA enhances macrophage autophagy by increasing mRNA expression of Atg5 and Atg16l1 and protein levels of LC3I and LC3II; electron microscopy confirmed that UA increases autophagosome formation in macrophages. However, the more detailed molecular mechanisms warrant further investigation; for example, what targets UA directly binds to in the cell or on the cell membrane, and how UA modulates Atg5 and Atg16l1 expression, but not several other autophagy-related genes.

Macrophages contribute to atherogenesis by serving as inflammatory machinery and as a lipid deposit tank. Autophagy has been shown to reduce macrophage inflammation and foam cell formation by various mechanisms. In the arm of inflammation in the arterial intima, oxidized lipids and other inflammatory stimuli provoke macrophages to produce a variety of inflammatory cytokines, including IL-1β, IL-6, and TNF-α, among which IL-1β plays a dominant role in the inflammatory cascade in the plaques. In this study, we show that UA significantly reduced intracellular pro-IL-1β levels and mature IL-1β secretion in LPS-treated macrophages, although it did not reduce IL-1β mRNA expression. Increasing evidence suggests that autophagy is necessary to keep down the endogenous sources of inflammasome and IL-1β activation (36). Macrophages derived from Atg16l1-deficient mice produced higher levels of IL-1β (9). Additional studies using cells of human origin demonstrated that the inhibition of autophagy led to the upregulated production of IL-1β (37, 38). To examine how UA regulates IL-1β production in macrophages, we used immunofluorescence confocal microscopy to observe colocalization of IL-1β and LC3 in Raw 264.7 cells after treatment by TLR ligands combined with UA. The overlap between IL-1β and LC3 indicated that autophagy induced by UA brought pro-IL-1β into the lumen of autophagic vacuoles for degradation, thereby reducing pro-IL-1β in the cells, which was usually processed by caspase 1 to generate mature IL-1β for secretion; although UA-induced autophagy did not suppress active caspase 1 generation through inflammasomes.

Oxidized or other modified LDL, unlike normal LDL, is readily taken up by the macrophage through scavenger receptors SR-A or CD36, resulting in the formation of macrophage foam cells. Accumulation of lipid-loaded macrophage foam cells is a central feature in the formation of atherosclerotic plaques (39, 40). Maintaining macrophage cholesterol homeostasis is essential for the prevention and treatment of atherosclerosis. In this study, we provide evidence that UA enhanced apoAI-mediated cholesterol efflux from macrophage foam cells through autophagy. Our data show that UA enhanced apoAI-mediated cholesterol efflux, which can be blocked by the autophagic flux inhibitor, bafilomycin A1.

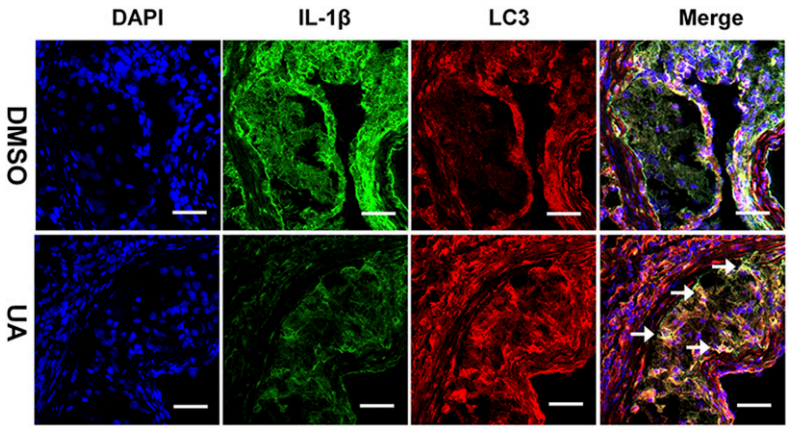

Fig. 5. UA increases IL-1β and LC3 colocalization in atherosclerotic lesions in mice. Representative fluorescent microscopic images for detecting LC3/IL-1β in aortic root sections are shown. The frozen tissue was stained with anti-LC3 and anti-IL-1β antibodies, as described in the Materials and Methods. White arrows indicate colocalization of LC3 and IL-1β. Scale bar: 200 μm.

By doing so, UA did not increase ABCA1 and ABCG1 expression; instead, UA increased lipophagy in macrophages, evidenced by the fusion of autophagosomes with LDs in the electron microscopic images. Our finding that enhanced autophagy is associated with improved cholesterol efflux from macrophages is consistent with previous reports (13, 14). It is worth noting that our electron microscopic images show that UA increased the frequency of LDs with areas of high density and asymmetrically localized multi-membrane structures. For larger LDs, autophagosomes only engulfed a discrete part of the LDs, which then pinched off as membrane vesicles enriched in LC3 (autolipophagosomes), in this way autophagosomes occur on the surface of these large organelles. Such partial engulfment of organelles by autophagy has been described for the nucleus and endoplasmic reticulum (41, 42).

We further demonstrate that the beneficial effects of UA on macrophage inflammatory response and cholesterol homeostasis translate well into atherosclerosis reduction in mouse models. We show that peritoneal injection of UA at 50 mg/kg once every other day in $LDLR^{-/-}$ mice fed a Western diet for 11 weeks significantly reduced atherosclerotic plaque formation. Detailed composition analysis for $LDLR^{-/-}$ mice showed that UA reduced the overall lesion size, the lipid containing area, and the macrophage content, while it increased the collagen content, suggesting that UA treatment results in smaller and more stable lesions in mice. Further immunohistochemical analysis revealed that UA treatment reduced IL-1β levels, but increased LC3 levels, in atherosclerotic plaque, and that UA significantly increased the colocalization of IL-1β and LC3 in the lesions, indicating that UA, indeed, reduced IL-1β concentration in plaque through enhancing autophagy and IL-1β sequestration and degradation in the autophagic pathway. ELISA data further confirmed the reduction of IL-1β in serum. These in vivo data demonstrate that the macrophage autophagy-inducing effects indeed confer UA with anti-atherogenic capacity.

There are two previous studies that investigated the effects of UA on atherosclerosis using mouse models that obtained opposite results. Ullevig et al. (31) showed that UA has anti-atherogenic effects on female $LDLR^{-/-}$ mice induced to be diabetic and fed a high fat diet supplemented with UA for 11 weeks. The mechanism was suggested to be monocyte recruitment suppression. Our results are in agreement with these findings because the absolute MOMA-2-stained area in the plaques of our $LDLR^{-/-}$ mice was reduced, although the area percentage reduction did not reach statistical significance. On the other hand, Messner et al. (43) reported a UA dose-dependent increase in atherosclerosis in Western diet-fed male $apoE^{-/-}$ mice receiving UA in drinking water for 24 weeks. The mechanisms were proposed to be endothelial cell death induction and serum IL-5 reduction caused by UA consumption. In our study, we did not examine the endothelial proliferation and apoptosis in UA-treated mice, but did not observe a significant decrease of serum IL-5 levels in $LDLR^{-/-}$ mice. As correctly pointed out by Tannock (44), all these studies, including ours, were designed differently, including the animal model, the UA administration route, the dose, and the duration, and the mechanistic studies evaluated different cell types. In our study, we administered UA using peritoneal injection, avoiding the potential metabolism of UA in the gut and first pass effects in the liver. The plasma UA concentration determined in mice was 3–12 μM within 24 h after a single injection, which is close to the concentrations we used in the in vitro macrophage experiments, indicating that the macrophage autophagy-enhancing mechanism identified in in vitro experiments can at least partially explain the anti-atherogenic effects. Indeed, we also directly observed enhanced autophagy in the plaques of UA-treated mice. Nevertheless, more studies are needed to confirm the effects of UA on atherosclerosis and to more comprehensively examine the mechanisms.

In conclusion, our data suggest that UA enhances macrophage autophagy and thus reduces pro-IL-1β processing into mature IL-1β, and promotes macrophage cholesterol efflux (as depicted in **Fig. 6**). Both of these effects are anti-atherogenic, contributing to the attenuated atherogenesis in $LDLR^{-/-}$ mice fed a Western diet. Our study provides evidence that UA might be an optimal anti-atherogenic therapy by virtue of its macrophage autophagy-enhancing activity.

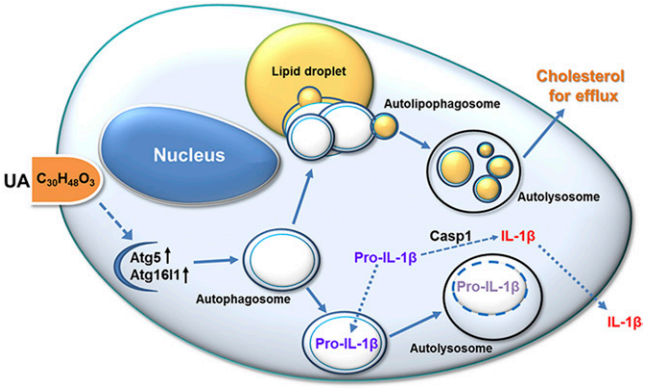

Fig. 6. Schematic depiction of the effects of UA on macrophages. UA enhances autophagy in macrophages by increasing expression of autophagy-related proteins Atg5 and Atg16l1. Autophagosome sequesters pro-IL-1β and leads to pro-IL-1β degradation in lysosomes, diverting it from being processed by caspase 1 into mature IL-1β for secretion. Autophagosomes also interact with LDs, encircling some lipids to form autolipophagosomes, and then fuse with the lysosome to form an autolysosome, which processes the containing lipids and presents FC to the cell membrane for ABCA1-mediated cholesterol efflux.

REFERENCES

1. Kundu, M., and C. B. Thompson. 2008. Autophagy: basic principles and relevance to disease. *Annu. Rev. Pathol.* **3:** 427–455.
2. Yang, Z., and D. J. Klionsky. 2010. Mammalian autophagy: core molecular machinery and signaling regulation. *Curr. Opin. Cell Biol.* **22:** 124–131.
3. Boya, P., F. Reggiori, and P. Codogno. 2013. Emerging regulation and functions of autophagy. *Nat. Cell Biol.* **15:** 713–720.
4. Martinet, W., P. Agostinis, B. Vanhoecke, M. Dewaele, and G. R. De Meyer. 2009. Autophagy in disease: a double-edged sword with therapeutic potential. *Clin. Sci. (Lond.).* **116:** 697–712.
5. Mizushima, N., B. Levine, A. M. Cuervo, and D. J. Klionsky. 2008. Autophagy fights disease through cellular self-digestion. *Nature.* **451:** 1069–1075.
6. Kroemer, G., G. Marino, and B. Levine. 2010. Autophagy and the integrated stress response. *Mol. Cell.* **40:** 280–293.
7. Levine, B., and G. Kroemer. 2008. Autophagy in the pathogenesis of disease. *Cell.* **132:** 27–42.
8. Füllgrabe, J., D. J. Klionsky, and B. Joseph. 2014. The return of the nucleus: transcriptional and epigenetic control of autophagy. *Nat. Rev. Mol. Cell Biol.* **15:** 65–74.
9. Saitoh, T., N. Fujita, M. H. Jang, S. Uematsu, B. G. Yang, T. Satoh, H. Omori, T. Noda, N. Yamamoto, M. Komatsu, et al. 2008. Loss of the autophagy protein Atg16L1 enhances endotoxin-induced IL-1beta production. *Nature.* **456:** 264–268.
10. Harris, J., M. Hartman, C. Roche, S. G. Zeng, A. O'Shea, F. A. Sharp, E. M. Lambe, E. M. Creagh, D. T. Golenbock, J. Tschopp, et al. 2011. Autophagy controls IL-1beta secretion by targeting pro-IL-1beta for degradation. *J. Biol. Chem.* **286:** 9587–9597.
11. Razani, B., C. Feng, T. Coleman, R. Emanuel, H. Wen, S. Hwang, J. P. Ting, H. W. Virgin, M. B. Kastan, and C. F. Semenkovich. 2012. Autophagy links inflammasomes to atherosclerotic progression. *Cell Metab.* **15:** 534–544.
12. Singh, R., S. Kaushik, Y. Wang, Y. Xiang, I. Novak, M. Komatsu, K. Tanaka, A. M. Cuervo, and M. J. Czaja. 2009. Autophagy regulates lipid metabolism. *Nature.* **458:** 1131–1135.
13. Ouimet, M., V. Franklin, E. Mak, X. Liao, I. Tabas, and Y. L. Marcel. 2011. Autophagy regulates cholesterol efflux from macrophage foam cells via lysosomal acid lipase. *Cell Metab.* **13:** 655–667.
14. Ouimet, M., and Y. L. Marcel. 2012. Regulation of lipid droplet cholesterol efflux from macrophage foam cells. *Arterioscler. Thromb. Vasc. Biol.* **32:** 575–581.
15. Liao, X., J. C. Sluimer, Y. Wang, M. Subramanian, K. Brown, J. S. Pattison, J. Robbins, J. Martinez, and I. Tabas. 2012. Macrophage autophagy plays a protective role in advanced atherosclerosis. *Cell Metab.* **15:** 545–553.
16. Bonilla, D. L., A. Bhattacharya, Y. Sha, Y. Xu, Q. Xiang, A. Kan, C. Jagannath, M. Komatsu, and N. T. Eissa. 2013. Autophagy regulates phagocytosis by modulating the expression of scavenger receptors. *Immunity.* **39:** 537–547.
17. Shashkin, P., B. Dragulev, and K. Ley. 2005. Macrophage differentiation to foam cells. *Curr. Pharm. Des.* **11:** 3061–3072.
18. Hansson, G. K., and P. Libby. 2006. The immune response in atherosclerosis: a double-edged sword. *Nat. Rev. Immunol.* **6:** 508–519.
19. Waldo, S. W., Y. Li, C. Buono, B. Zhao, E. M. Billings, J. Chang, and H. S. Kruth. 2008. Heterogeneity of human macrophages in culture and in atherosclerotic plaques. *Am. J. Pathol.* **172:** 1112–1126.
20. Shimada, K. 2009. Immune system and atherosclerotic disease: heterogeneity of leukocyte subsets participating in the pathogenesis of atherosclerosis. *Circ. J.* **73:** 994–1001.
21. Swirski, F. K., R. Weissleder, and M. J. Pittet. 2009. Heterogeneous in vivo behavior of monocyte subsets in atherosclerosis. *Arterioscler. Thromb. Vasc. Biol.* **29:** 1424–1432.
22. Tabas, I. 2010. Macrophage death and defective inflammation resolution in atherosclerosis. *Nat. Rev. Immunol.* **10:** 36–46.
23. Maiuri, M. C., G. Grassia, A. M. Platt, R. Carnuccio, A. Ialenti, and P. Maffia. 2013. Macrophage autophagy in atherosclerosis. *Mediators Inflamm.* **2013:** 584715.
24. Morrisett, J. D., G. Abdel-Fattah, R. Hoogeveen, E. Mitchell, C. M. Ballantyne, H. J. Pownall, A. R. Opekun, J. S. Jaffe, S. Oppermann, and B. D. Kahan. 2002. Effects of sirolimus on plasma lipids, lipoprotein levels, and fatty acid metabolism in renal transplant patients. *J. Lipid Res.* **43:** 1170–1180.
25. Martinet, W., I. De Meyer, S. Verheye, D. M. Schrijvers, J. P. Timmermans, and G. R. De Meyer. 2013. Drug-induced macrophage autophagy in atherosclerosis: for better or worse? *Basic Res. Cardiol.* **108:** 321.
26. Ali, M. S., S. A. Ibrahim, S. Jalil, and M. I. Choudhary. 2007. Ursolic acid: a potent inhibitor of superoxides produced in the cellular system. *Phytother. Res.* **21:** 558–561.
27. Ikeda, Y., A. Murakami, and H. Ohigashi. 2008. Ursolic acid: an anti-cancer and pro-inflammatory triterpenoid. *Mol. Nutr. Food Res.* **52:** 26–42.
28. Somova, L. O., A. Nadar, P. Rammanan, and F. O. Shode. 2003. Cardiovascular, antihyperlipidemic and antioxidant effects of oleanolic and ursolic acids in experimental hypertension. *Phytomedicine.* **10:** 115–121.
29. Jayaprakasam, B., L. K. Olson, R. E. Schutzki, M. H. Tai, and M. G. Nair. 2006. Amelioration of obesity and glucose intolerance in high-fat-fed C57BL/6 mice by anthocyanins and ursolic acid in Cornelian cherry (Cornus mas). *J. Agric. Food Chem.* **54:** 243–248.
30. Kunkel, S. D., C. J. Elmore, K. S. Bongers, S. M. Ebert, D. K. Fox, M. C. Dyle, S. A. Bullard, and C. M. Adams. 2012. Ursolic acid increases skeletal muscle and brown fat and decreases diet-induced obesity, glucose intolerance and fatty liver disease. *PLoS One.* **7:** e39332.
31. Ullevig, S. L., Q. Zhao, D. Zamora, and R. Asmis. 2011. Ursolic acid protects diabetic mice against monocyte dysfunction and accelerated atherosclerosis. *Atherosclerosis.* **219:** 409–416.
32. Leng, S., Y. Hao, D. Du, S. Xie, L. Hong, H. Gu, X. Zhu, J. Zhang, D. Fan, and H. F. Kung. 2013. Ursolic acid promotes cancer cell death by inducing Atg5-dependent autophagy. *Int. J. Cancer.* **133:** 2781–2790.
33. Liang, Q., Q. Wu, J. Jiang, J. Duan, C. Wang, M. D. Smith, H. Lu, Q. Wang, P. Nagarkatti, and D. Fan. 2011. Characterization of sparstolonin B, a Chinese herb-derived compound, as a selective Toll-like receptor antagonist with potent anti-inflammatory properties. *J. Biol. Chem.* **286:** 26470–26479.
34. Yu, F., F. Du, Y. Wang, S. Huang, R. Miao, A. S. Major, E. A. Murphy, M. Fu, and D. Fan. 2013. Bone marrow deficiency of MCPIP1 results in severe multi-organ inflammation but diminishes atherogenesis in hyperlipidemic mice. *PLoS One.* **8:** e80089.
35. Du, F., F. Yu, Y. Wang, Y. Hui, K. Carnevale, M. Fu, H. Lu, and D. Fan. 2014. MicroRNA-155 deficiency results in decreased macrophage inflammation and attenuated atherogenesis in apolipoprotein E-deficient mice. *Arterioscler. Thromb. Vasc. Biol.* **34:** 759–767.
36. Jiang, S., N. Dupont, E. F. Castillo, and V. Deretic. 2013. Secretory versus degradative autophagy: unconventional secretion of inflammatory mediators. *J. Innate Immun.* **5:** 471–479.

37. Shin, S. W., S. Y. Kim, and J. W. Park. 2012. Autophagy inhibition enhances ursolic acid-induced apoptosis in PC3 cells. *Biochim. Biophys. Acta.* **1823:** 451–457.
38. Plantinga, T. S., T. O. Crisan, M. Oosting, F. L. van de Veerdonk, D. J. de Jong, D. J. Philpott, J. W. van der Meer, S. E. Girardin, L. A. Joosten, and M. G. Netea. 2011. Crohn's disease-associated ATG16L1 polymorphism modulates pro-inflammatory cytokine responses selectively upon activation of NOD2. *Gut.* **60:** 1229–1235.
39. Moore, K. J., and I. Tabas. 2011. Macrophages in the pathogenesis of atherosclerosis. *Cell.* **145:** 341–355.
40. Moore, K. J., F. J. Sheedy, and E. A. Fisher. 2013. Macrophages in atherosclerosis: a dynamic balance. *Nat. Rev. Immunol.* **13:** 709–721.
41. Roberts, P., S. Moshitch-Moshkovitz, E. Kvam, E. O'Toole, M. Winey, and D. S. Goldfarb. 2003. Piecemeal microautophagy of nucleus in Saccharomyces cerevisiae. *Mol. Biol. Cell.* **14:** 129–141.
42. Bernales, S., K. L. McDonald, and P. Walter. 2006. Autophagy counterbalances endoplasmic reticulum expansion during the unfolded protein response. *PLoS Biol.* **4:** e423.
43. Messner, B., I. Zeller, C. Ploner, S. Frotschnig, T. Ringer, A. Steinacher-Nigisch, A. Ritsch, G. Laufer, C. Huck, and D. Bernhard. 2011. Ursolic acid causes DNA-damage, p53-mediated, mitochondria- and caspase-dependent human endothelial cell apoptosis, and accelerates atherosclerotic plaque formation in vivo. *Atherosclerosis.* **219:** 402–408.
44. Tannock, L. R. 2011. Ursolic acid effect on atherosclerosis: apples and apples, or apples and oranges? *Atherosclerosis.* **219:** 397–398.